Revealing dominant patterns of aerosols regimes in the lower troposphere and their evolution from preindustrial times to the future in global climate model simulations

Jingmin Li[1], Mattia Righi[1], Johannes Hendricks[1], Christof G. Beer[1], Ulrike Burkhardt[1], Anja Schmidt[1,2,3]

5 [1]Deutsches Zentrum für Luft- und Raumfahrt (DLR), Institut für Physik der Atmosphäre, Oberpfaffenhofen, Germany
[2]Meteorological Institute, Ludwig Maximilian University of Munich, Munich, Germany
[3]Yusuf Hamied Department of Chemistry, University of Cambridge, Cambridge, United Kingdom

Correspondence to: Jingmin Li (Jingmin.Li@dlr.de)

10 **Abstract.** Aerosols play an important role in the Earth system, but their impact on cloud properties and the resulting radiative forcing of climate remains highly uncertain. The large temporal and spatial variability of a number of aerosols properties and the choice of different 'pre-industrial' reference years prevent a concise understanding of basic underlying patterns and trends in aerosols and their impacts on clouds and radiation. In this study, we characterize the spatial patterns and long-term evolution of lower tropospheric aerosols (in terms of regimes) by clustering multiple aerosol properties from preindustrial times to the

15 year 2050 under three different Shared Socioeconomic Pathway (SSP) scenarios, based on a combination of global aerosol model simulations and statistic-based machine learning algorithms. Our analysis suggests that in comparison with the present-day case, lower tropospheric aerosol regimes during preindustrial times are mostly represented by regimes of comparatively clean conditions whereby marked differences between the years 1750 and 1850 emerge due to the growing influence of agriculture and other anthropogenic activities in 1850. Key aspects of the spatial distribution and extent of the aerosol regimes

20 identified in year 2050 differ compared to pre-industrial and present-day, with significant variations resulting from the emission scenario investigated. In 2050, the low emission SSP1-1.9 scenario is the only scenario where the spatial distribution and extent of the aerosol regimes very closely resembles preindustrial conditions whereby the similarity is greater compared to 1850 than 1750. The aerosol regimes for 2050 under SSP3-7.0 closely resemble present-day conditions, but there are some notable regional differences: developed countries tend to shift towards cleaner conditions in future, while the opposite is the

25 case for developing countries. The aerosol regimes for 2050 under SSP2-4.5 represent an intermediate stage between preindustrial times and present-day. Further analysis indicates a north/south difference in the background regime during preindustrial times, and close resemblance of pre-industrial aerosol conditions in the marine regime to present-day conditions in the Southern Hemispheric ocean. Overall, our study allows to extract a clear and condensed picture of the spatial extent and distribution of aerosols for different time periods and emission scenarios and to summarize these in terms of aerosol regimes.

30 The approach and findings of this study can be used for designing targeted measurements of different preindustrial-like conditions, and for tailored air pollution mitigation measures in specific regions.

1 Introduction

Aerosols play an important role in the Earth's climate, by direct scattering and absorption of solar and terrestrial radiation (termed aerosol-radiation interactions), and indirect effects due to modifications of cloud microphysical and radiative

35   properties (termed aerosol-cloud interactions) (Boucher et al., 2013). Aerosols influence the climate system in different ways and show a large spatial and temporal variability due to the large variety of aerosol species, mixing states, residence times and size ranges in the atmosphere (e.g. Lauer and Hendricks 2006; Mann et al., 2010; Pringle et al., 2010; Sessions et al., 2015). Aerosols also affect air quality, human health, and visibility as well as regional and global temperature and precipitation patterns, whereby many of these interactions between aerosols, air quality and climate remain uncertain (Kulmala et al. 2011,

40   Myhre et al 2017, Bellouin et al 2020).

In order to reduce uncertainties on aerosol-climate interactions, it is vital to gain better knowledge of the temporal and spatial evolution of aerosols over time. The preindustrial period is considered as a baseline for radiative forcing calculations, but different definitions can be found in the literature, using the year 1750 or 1850. Quantifying preindustrial aerosol conditions

45   is essential for evaluating the magnitude of radiative forcing caused by anthropogenic aerosols (Andreae, 2007). Carslaw et al. (2013) investigated uncertainties in present-day aerosol indirect radiative forcing resulting from aerosol-cloud interactions, and demonstrated that 45% of the variance in the magnitude of the aerosol indirect forcing is explained by natural emissions while only 34% is explained by anthropogenic emissions. Therefore, it is important to obtain precise information about preindustrial aerosol conditions. Gryspeerdt et al. (2023) demonstrated that the uncertainty in aerosol-cloud radiative forcing

50   is driven by clean aerosol conditions, and suggested constraining aerosol properties in clean conditions as an important goal for future observational studies. Efforts have been made to identify regions on Earth with aerosol properties similar to those during the preindustrial period. Based on modeling studies, such preindustrial aerosol conditions (defined as an overall picture of aerosol properties at that time) can be found mostly over present-day oceanic regions in the Southern Hemisphere (Andreae, 2007; Carslaw et al., 2014; Hamilton et al., 2014; McCoy et al., 2020). Hence, aerosol measurements over the remote Southern

55   oceans can be used to constrain aerosol radiative forcing uncertainties (Schmale et al., 2019; Regayre et al., 2020). On the other hand, aerosols play also an important role in future climate projections (IPCC 2021; Quaas et al. 2022). Andreae et al. (2005) suggest that the strong cooling effect induced by aerosols in the past and present climate could decrease in the future, depending on the temporal and spatial evolution of aerosol emissions. Xu et al. (2018) studied the importance of aerosol scenarios in predicting future heat extremes and demonstrated that aerosols are more important than greenhouse gases in

60   controlling heat extreme statistics over Northern Hemisphere extra-tropical land areas and the duration of heat extremes in the tropics. A further modelling study by Zhao et al. (2019) suggests that future anthropogenic aerosol changes can significantly affect future heatwave predictions. Overall, it is therefore essential to classify aerosol properties and hence characterize aerosol conditions under different future emission scenarios compared with pre-industrial times and the present-day.

65 Here we use the output of the global aerosol-chemistry-climate model EMAC (ECHAM/MESSy Atmospheric Chemistry) equipped with the aerosol microphysical sub-module MADE3 (the third generation of the Modal Aerosol Dynamics model for Europe adapted for global applications), together with statistic-based clustering algorithms to characterize similarities and differences in aerosol properties from preindustrial times to the present-day and the future (year 2050). In contrast to previous studies that primarily investigated preindustrial aerosol conditions based on a single parameter - cloud condensation nuclei

70 (CCN) - within the context of aerosol-cloud interaction (e.g. Andreae 2007, Hamilton et al. 2014), the method proposed here combines multiple aerosol properties and targets different time periods. The aerosol properties considered in our study are derived from EMAC-MADE3 model-simulated quantities and include mass concentrations of black carbon (BC), particulate organic matter (POM), mineral dust, sea salt, aerosol sulfate, ammonium, nitrate, and particle number concentrations in the Aitken and accumulation modes. Analysing all these variables individually across different time periods would result in

75 numerous different aerosol distribution patterns, which makes it impossible to draw universal conclusions. In this context, clustering of the multivariate aerosol data provides us with an aggregated and condensed picture of aerosol regimes and their evolution. In our previous study (Li et al. 2022; hereafter L22), we successfully defined present-day global aerosol regimes and analysed their internal characteristics regarding the individual aerosol properties (e.g., concentrations of specific aerosol species) for each regime, using the unsupervised machine learning algorithm K-means. In the present study, we use the

80 approach of L22 for defining global aerosol regimes (hereafter termed primary classification), and further extend the procedure to also investigate finer structures within specific aerosol regimes (hereafter termed secondary classification), and we investigate the temporal evolution of the regimes from the preindustrial period to the year 2050 with further developed analyses procedures. The goal of the primary classification is to characterize the variability range and relative difference of aerosol properties across the globe, while the secondary classification is used to characterize each specific regime in more detail. The

85 clustering method used in L22, however, was designed for a single time slice and cannot be used for different time periods, as it would lead to incomparable regimes due to the different aerosol conditions in different time periods. More specifically, aerosol conditions during preindustrial times do not agree with the present-day, due to additional contributions from anthropogenic emissions. For the present study, we therefore additionally include the supervised Random Forest machine learning algorithm (Ho 1995, Breiman 2001). As a supervised method, the Random Forest algorithm can be trained using data

90 for one specific time slice and applied to all other time slices. In this way, all time slices are analysed consistently and the temporal evolution of the aerosol regimes can be studied. We focus here only on the lower troposphere (from the surface to about 700 hPa), where the aerosol regimes are strongly connected to the emission patterns.

Overall, we aim to address the following questions: (1) How do aerosol regimes develop over time, from pre-industrial times

95 (years 1750 and 1850) to the future (year 2050) under different emission scenarios? (2) Where can aerosol conditions similar to preindustrial times be found in the present-day and future? (3) What is the effect of different emission pathways on the development of the aerosol regimes? Answering these questions can help to target measurements for specific aerosol conditions (e.g. preindustrial-like or highly polluted), to supply information to policy makers (e.g. emission mitigation efforts in specific

scenarios and their expected effects), to provide important hints for subsequent studies relying on information about the
100 properties and distribution of atmospheric aerosols (e.g. evaluating environmental impacts of particulate matter).

2 Methodology

2.1 Global model simulations and data

In this study, we investigate the development of global aerosol regimes based on simulations using a global aerosol-chemistry-climate model for four climatological time slices and three future scenarios. These comprise preindustrial times (1750 and
105 1850), present day (2015), and future (2050) under three different emission scenarios of the Shared Socioeconomic Pathways (SSPs; O'Neill et al., 2017; Gidden et al., 2017): SSP1-1.9, SSP2-4.5 and SSP3-7.0. SSP1-1.9 is a low emission scenario, projecting close to net-zero carbon dioxide (CO_2) emissions by 2050 and a temperature rise of 1.4 K by the end of the century. SSP2-4.5 is a middle-of-the-road scenario, with CO_2 emissions staying at current level until 2050 and decreasing afterwards, resulting in a temperature rise of 2.7 by 2100. SSP3-7.0 is a pessimistic scenario, projecting a doubling of CO_2 levels and 3.6
110 K temperature rise by 2100 (IPCC, 2021). We investigate both year 1750 and year 1850 preindustrial conditions. The year 1750 is commonly considered as the preindustrial reference case by several studies (e.g. Boucher et al 2013; Hamilton et al. 2014; Hawkins et al 2017; IPCC 2021), while other studies (e.g., Carslaw et al., 2017) argued that the year 1850 should be used as a preindustrial reference period when considering aerosol radiative forcing because the year 1850 shows marked difference in terms of aerosol emissions compared to 1750. The IPCC Special Report on Global Warming of 1.5°C (IPCC
115 2022) uses the period 1850–1900 as preindustrial baseline.

The simulations analysed in this study were performed as part of an assessment of the global impact of the emissions of the transport sector on aerosol and climate (Righi et al., 2023), using the ECHAM/MESSy Atmospheric Chemistry (EMAC) general circulation model (Jöckel et al., 2010, 2016) equipped with the aerosol microphysical sub-module MADE3 (Kaiser et
120 al., 2014, 2019). It simulates nine different aerosol species: BC, POM, ammonium, sulfate, nitrate, the sea salt species sodium and chloride, mineral dust and aerosol water. These nine species are distributed into three different mixing states within three size ranges, resulting in a total of nine aerosol modes for each species. The three mixing states include purely soluble particles, particles mainly composed of insoluble material and only very thin soluble coatings (<10% of the total particle mass), and mixed particles consisting of an insoluble core with a soluble coating. The three size modes are Aitken-, accumulation- and
125 coarse mode. MADE3 considers particle microphysical changes due to condensation, coagulation, gas-particle partitioning and new particle formation. MADE3 was proven to be able to properly represent aerosol microphysical processes, with the simulated aerosol properties showing good agreement with observations, as demonstrated in previous studies (Kaiser et al., 2014; Kaiser et al. 2019; Beer et al., 2020; Righi et al., 2020).

130 All simulations are performed in the T42L41 resolution, corresponding to a grid of 2.8°×2.8° in latitude and longitude and 41 vertical hybrid σ-pressure levels up to 5 hPa. In this study, we only consider changes in the emissions of short-lived species (aerosols and aerosol precursor gases) for the different time slices, while the climate is held constant at present-day conditions. Due to the complexity and interactions of microphysical processes in the global aerosol climate model, it would be difficult to distinguish the influence of climate change and emission changes if both would be considered at the same time and our major

135 goal is to link the development of global aerosol regimes through time to the emission patterns. Moreover, L22 demonstrated that emissions are the key drivers for global aerosol regimes, especially for the lower troposphere. Additionally, Koffi et al (2010) showed that the effect of emission changes on transport-induced ozone is larger than the effect of climate change, providing a hint that aerosols could be more influenced by emission than climate. For this reason, EMAC is applied in nudged mode, i.e. model dynamics are constrained using ERA-Interim reanalysis data (Dee et al., 2011), more specifically,

140 temperature, wind divergence and vorticity, and the logarithm of the surface pressure for the time period used to constrain the climate (2006-2015). The emission data applied for preindustrial times, present-day conditions, and future scenarios are taken from the CMIP6 inventory (van Marle et al 2017, Hosely et al 2018, Gidden et al 2019, Feng et al. 2020), including natural and anthropogenic particulate and gas emissions from different sectors such as biomass burning (BB), agricultural waste burning (AWB), land transport, shipping, aviation, and other anthropogenic sources. Since the emissions of mineral dust and

145 sea salt are wind-driven, they are calculated online for each model time step using the parameterizations by Tegen et al. (2002) and by Guelle et al. (2001), for mineral dust and sea salt, respectively.

The development of aerosol regimes over time is analyzed on a climatological mean basis. Aerosol properties for the machine learning classification tasks are extracted from multi-annual average (10 year) simulation data. As in L22, the clustering

150 algorithm considers seven aerosol properties: aerosol mass concentrations of BC, mineral dust, sea salt, POM, the sum of sulfate, nitrate, and ammonium (SNA), as well as number concentrations of aerosol particles in the Aitken and accumulation modes. To characterize aerosol regimes in the lower troposphere, the simulated mass and number concentrations are vertically integrated between the terrain-following hybrid sigma pressure levels 41 (corresponding to the surface) to 33 (corresponding to an altitude range from the ground to about 700 hPa).

155 **2.2 Description of machine learning classification methods in general**

In this study, we apply two statistic-based machine learning algorithms that compare and evaluate the similarity and differences among different datasets: the unsupervised K-means clustering and the supervised Random Forest classifier.

K-means (MacQueen 1967, Hartigan and Wong 1979) is an unsupervised machine learning clustering algorithm, which has

160 been applied in several recent atmospheric modeling studies (e.g., Borge et al., 2022; Li et al., 2022; Raudesepp and Maljutenko, 2022). Unsupervised methods require no prior classification knowledge, but need a labeling and evaluating of the results after the classification. K-means can divide an input dataset into a predefined number of clusters using an equal variance

criterion. K-means is based on the calculation of Euclidean distance (Spencer, 2013) which computes the distance between two samples in a multi-dimensional space (with the number of dimensions equal to the number of variables). K-means can

165   perform clustering for a predefined number of clusters, but does not provide information about the optimal number of clusters to be used. Many classification evaluation metrics (e.g. Rousseeuw, 1987; Tibshirani et al. 2001) can support the selection of an optimal number but there is no general solution for all cases. The input dataset should be standardized for K-means classification, to overcome the problem of input variable values spanning different orders of magnitude, which leads to that input variables are not equally weighted (see L22, for details). The choice of an appropriate scaling method depends on the

170   input dataset and on the application (Milligan and Cooper, 1988).

Random Forest is a supervised machine learning method. A detailed description of Random Forest classification can be found in Ho (1995) and Breiman (2001). Briefly, Random Forest requires a preexisting classification of the input data in order to learn decision rules. Random Forest uses an ensemble learning technique that performs the classification by creating an

175   ensemble of decision trees: the so called 'forest'. The majority of votes from all decisions is considered as the final output. Compared to a single decision tree, this type of ensemble classification improves the performance and avoids the tendency of a single tree to overfit its training dataset (Hastie et al., 2008). Decision trees (Quinlan, 1986; Quinlan, 1987) are the basis of a Random Forest. Each decision tree is built by using a unique subset of samples randomly collected from the training data. A decision tree simulates intelligent behavior and has the ability to learn. The decision tree is built with a tree structure including

180   root node, decision nodes, and leaf nodes. All nodes are connected with branches. The paths from the root node to leaf nodes are controlled by decision rules. Decision notes contain decisive questions, yes/no-answers of these depicting questions lead the decision path to different branches. Depending on how the respective sequences of questions were answered in the decision trees and how the respective branches reach the leaf nodes, a set of class labels is generated. Random Forest is among the best supervised learning algorithms in terms of accuracy and performance (Liaw and Wienner, 2002) and has been widely used in

185   aerosols studies (e.g., Wei et al., 2010; Christopoulos et al., 2018; Choi et al., 2021; Kianian et al., 2021; Lee et al., 2021; Yu et al., 2022).

2.3 Analysis and applied classification approach

The analysis and classification approach applied in this study is based on the K-Means algorithm as in L22 and further extended with the Random Forest algorithm. The latter is required due to the equal variance criterion implemented in the K-means

190   algorithm (Hartigan and Wong, 1979), which would lead to the identification of incomparable regimes across the different time periods when performing K-means classification for each time period independently. Furthermore, applying K-means to a combined dataset of all the different time periods leads to comparable regimes across all time periods, but the classification results change whenever a new time period or scenario is considered. To overcome these limitations, we developed a two-step approach using a combination of K-means and Random Forest, which is outlined schematically in Fig. 1. First, we choose

195   present-day (REF-2015) as our reference time period and apply the L22 procedures to this reference time. Next, we apply the

Random Forest classification rules learned from REF-2015 and apply these rules to all other time periods in order to generate comparable and consistent aerosol regimes. This, in turn, allows us to identify present-day and future aerosol regimes that have a high probability to feature aerosol conditions that are similar to those during the pre-industrial period.
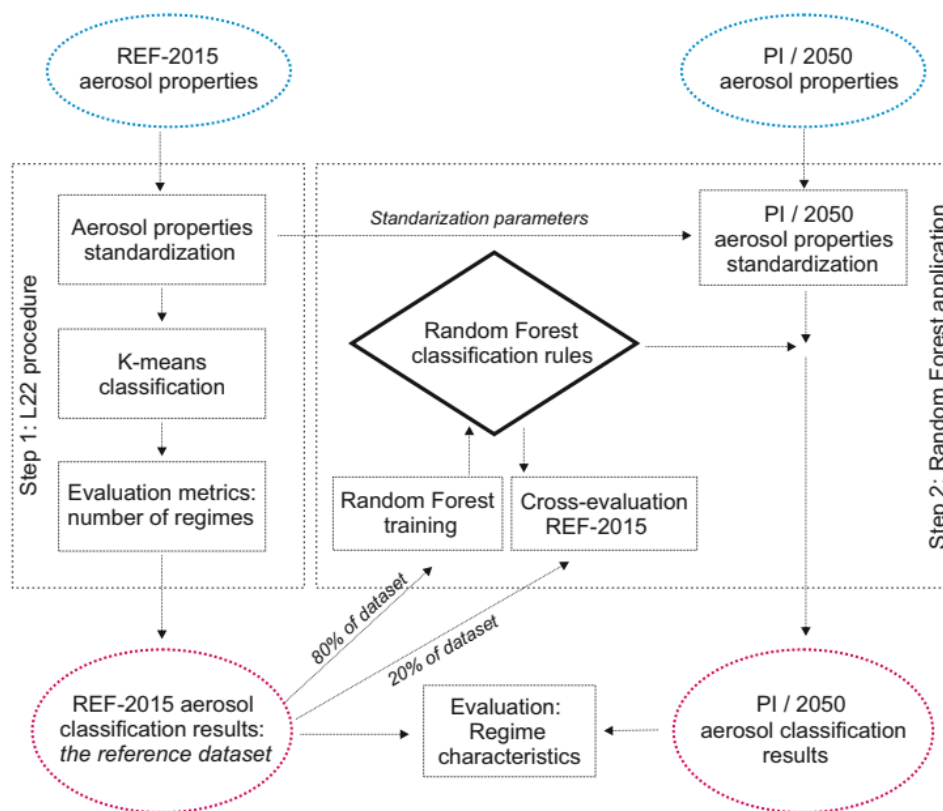
200

Figure 1: Workflow of applied machine learning classification procedures. Blue ovals represent the input data. Red ovals show the output data. Rectangles represent procedures to analyze the data. Diamond represents decision rules. Arrows show the sequence of analysis.

205

The global aerosol classification for present-day conditions (REF-2015) follows exactly the same procedures as shown in L22, including aerosol properties standardization, K-means classification, and evaluation for the choice of the final number of regimes. The values of the REF-2015 input aerosol properties are standardized before applying K-means in order to be equally weighted by the algorithm. We use the most suitable standardization method for global aerosol classification, which is based on sample mean and sample standard deviation. More specifically, each aerosol property is standardized by subtracting its sample mean and dividing the difference by its sample standard deviation. K-means classification is conducted for a range of

defined numbers of regimes. The choice of the optimal number of aerosol regimes is based on two evaluation metrics (the sum of squared errors and the silhouette coefficient). The L22 procedure applied to the REF-2015 data generates a sample dataset containing the values of the considered aerosol properties and the assigned regime index for each individual model grid point

215 (a dataset of 8192 points resulting from 128 longitude and 64 latitude grid points). This dataset is considered the 'ground truth' for the following machine learning processes and serves as the training dataset for the supervised machine learning with the Random Forest classifier in the second step of our procedure.

The Random Forest classifier has the ability to learn how to make decisions for specific aerosol regimes based on the training

220 data generated for REF-2015 using K-means. The input properties for all other time slices are standardized consistently using their corresponding REF-2015 standardization parameters (mean and standard deviation) to create consistent inputs for the Random Forest algorithm. A cross-validation process is applied to the Random Forest learning by selecting 80% of the REF-2015 data points, which the algorithm uses to learn the aerosol classification decision rules. The evaluation is conducted for the remaining 20% of REF-2015 data points which are excluded from the learning process, by comparing aerosol regime labels

225 generated by the Random Forest decision rules to the original K-means classification. The resulting accuracy of the Random Forest classifier ranges between 94.5% and 98.8%, and is therefore well-suited for the analysis conducted in this study. The accuracy of the Random Forest algorithm is also evaluated, by comparing the internal properties of the aerosol regimes in REF-2015 generated by K-means and those of the other time slices generated by Random Forest (Sect. 3.1). The above procedures are applied for both the primary and secondary classification for the following reasons: 1) The classification of the

230 full global data set (primary classification) can identify aerosol regimes that, on a global scale, are characterized by marked difference in aerosol properties. In detail, the global data span a wide range of values and aerosol properties, which are distributed quite heterogeneously over the globe. Due to this large variability in the global dataset, the primary classification identifies regimes with clear difference, e.g. regimes containing high local values for specific aerosol species and regimes where the values of aerosol properties are close to their global minimum (hereafter termed clean aerosol regimes), however it

235 cannot further distinguish differences within the clean regimes. We therefore conduct a secondary classification to investigate fine structures within clean aerosol regimes, using the same procedure as for the primary classification, but applied to a subset of the data representative of a specific primary aerosol regime. With the secondary classification we zoom into a specific aerosol regime and can identify further detailed differences within it. The secondary classification is of special importance for the analysis of preindustrial regimes or future regimes under low pollution scenarios, such as SSP1-1.9, where clean aerosol

240 regimes dominate.

3 Results and discussions

3.1 Primary classification of aerosol regimes and their properties

Before discussing the development of primary classification aerosol regimes over time, it is important to distinguish the regime differences caused by numerical artifacts of the algorithm from the real regime changes in the model simulations. First, we

245 need to evaluate whether the aerosol regimes identified across the other time periods by the Random Forest algorithm agree with the present-day ones as classified by K-means (i.e., the 'ground truth' for Random Forest learning). The comparison of aerosol properties for the identified primary classification aerosol regimes across time periods (Fig. S1 in the Supplementary Material) shows that similar internal aerosol properties are derived for each identified aerosol regime from primary classification between REF-2015 and the preindustrial and future time periods. This suggests that Random Forest correctly

250 learns the classification criteria and is well suited for this study. One minor discrepancy between the two algorithms is the classification of the dust-dominated regimes: the data distributions of the dust-dominated level 1 regime in the preindustrial and in SSP1-1.9 is characterized by many outliers compared with the distribution in REF-2015, which should instead be assigned to the dust-dominated level 2 regime. This discrepancy is due to the fact that K-means is based on the Euclidean distance and is therefore more sensitive to the large values of a distribution, while Random Forest is less sensitive to them as

255 it predicts classes in a tree structure. This discrepancy suggests that it would be more appropriate to discuss the two dust-dominated regimes as a single one. Considering also that the dust-dominated level 2 regime is small in terms of sample size, the differences between these two regimes should not be over-emphasized.
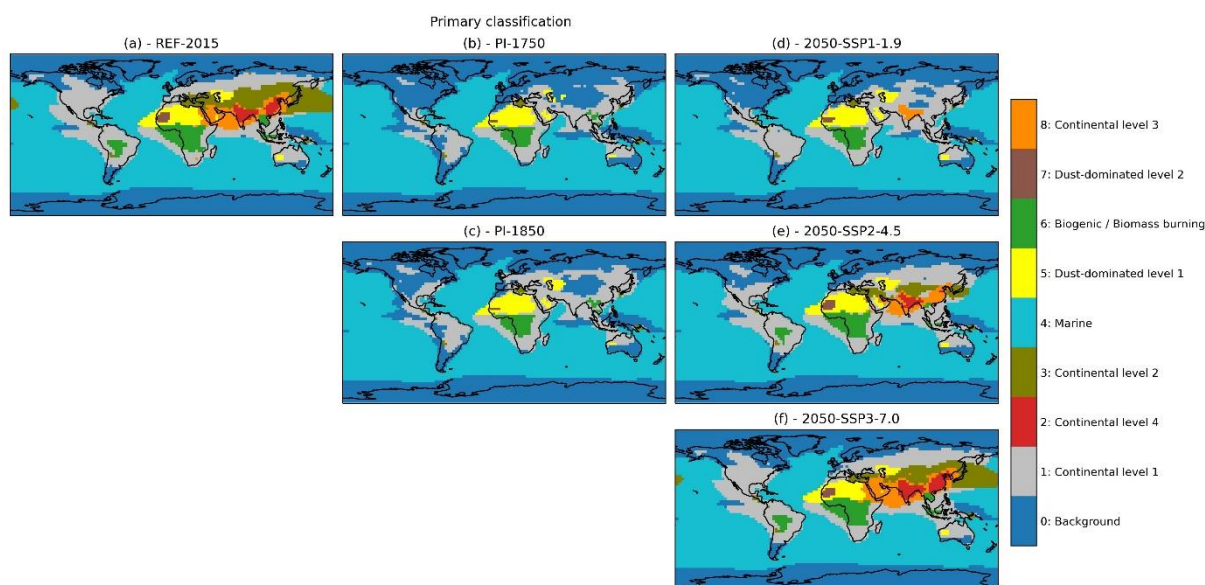
260 **Figure 2: Present-day (a), preindustrial times (b-c) and future (d-f) aerosol regimes from primary classification. The aerosol properties of each present-day regime are shown in Fig. 3.**

In the following, we first discuss the identified present-day primary classification aerosol regimes (Fig. 2) and their properties
(Fig. 3), then discuss these for the preindustrial cases and the future. Figures 2a and 3 show that there is a background regime

265 in the polar regions (regime 0), where all aerosol properties show lower values than the other regimes. The marine regime
(regime 4) is dominated by an enhancement in sea salt, while all other aerosol properties show only low values. Regimes 5
and 7 are dust-dominated regimes located over the Sahara. Regime 6 can be related to biomass burning activity/biogenic
emissions in forest regions and savannas of South America and Africa and the respective downwind areas. In addition, regime
6 is characterized by a clear enhancement in POM, BC and particle number concentration in the accumulation mode, which is

270 typical of this emission source. Four different continental regimes are identified, which are characterized by different levels of
aerosol due to anthropogenic influences (Regime 1, 3, 8, and 2, hereafter referred to continental level 1 to level 4 regimes,
respectively, in increasing order of anthropogenic influences).

275
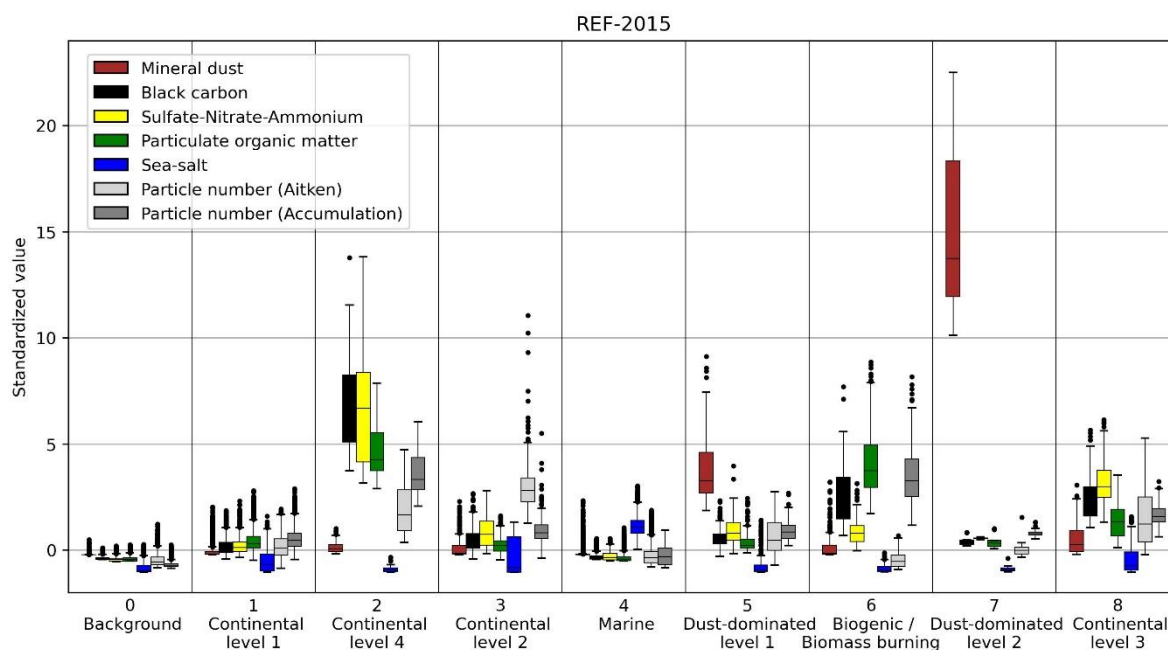
Figure 3: Internal aerosol properties of the primary classification aerosol regimes shown in Fig. 2. The boxes mark the range of data between the 25% and 75% quantiles, referring to the interquartile range (IQR). The whiskers indicate the minimum and maximum value within the 1.5×IQR distance from the box. Data beyond the whiskers are displayed as dots. The raw input values are standardized by removing the sample mean and dividing by the sample standard deviation, this standardization procedure preserves
280 **the data distribution and changes only data values. The standardized value 0 represents the global average of each aerosol property. The negative (positive) standardized values describe data below (above) global average expressed as factors of their global standard deviation.**

The aerosol regimes in preindustrial times (Fig. 2b, c) are mostly characterized by three clean primary classification aerosol
285   regimes (background, marine, and continental level 1) covering the whole globe. The spatial extent of the background regime
in preindustrial times is considerably larger than for present-day, covering large parts of the continents in the Northern and
Southern Hemisphere. The dust-dominated (regimes 5 and 7) and the biomass burning/biogenic regimes (regime 6) over Africa
exist throughout all time periods, although the spatial extent of the biomass burning/biogenic regime over Africa in
preindustrial times and in SSP1-1.9 is smaller than during the present-day. This indicates that the spatial extension of biomass
290   burning / biogenic regime in preindustrial times can be considered as a natural emission baseline, with the anthropogenic
contributions at present-day amplifying the biomass burning / biogenic regime to cover a larger area. The biomass burning
regime over South America, however, is not present in preindustrial times, suggesting the anthropogenic origin of the biomass
burning activity apart from agriculture in this region. Differences between the primary continental level 1 regimes emerge
between the two preindustrial time periods (PI-1750 and PI-1850), due to the growing influence of agriculture and other
295   anthropogenic activities between these two time periods. For example, North America, Europe and northern Asia belong to
the background regime (regime 0) in PI-1750, but shift to continental level 1 (regime 1) in PI-1850 with implications for the
choice of a representative year for preindustrial conditions when calculating aerosol radiative forcing (e.g. Carslaw et al. 2017;
IPCC 2022).

300   Key aspects of the spatial distribution and extent of the primary classification aerosol regimes in the future differ compared to
pre-industrial and present-day, with significant variations across the three SSP scenarios investigated here. SSP1-1.9 is the
scenario under which the primary classification aerosol regimes are most similar to 1750 or 1850. Under the low (SSP1-1.9,
Fig. 2d) and moderate (SSP2-4.5, Fig. 2e) emission scenarios, the shift towards preindustrial conditions is evident globally,
suggesting a general reduction of aerosol and aerosol precursor emissions in line with the underlying assumptions in these
305   scenarios (van Vuuren et al. 2017; Fricko et al. 2017). The spatial extent of continental level 2 to level 4 regimes (regimes 3,
8, and 2) is reduced under the SSP2-4.5 scenario, and these regimes disappear almost completely under SSP1-1.9. The low
emission SSP1-1.9 scenario is the only scenario where the spatial distribution and extent of the primary classification aerosol
regimes very closely resembles preindustrial conditions, whereby the agreement is larger for PI-1850 than PI-1750, except for
India that still belongs to the continental level 3 regime (regime 8). The scenario with most similarities with the present-day
310   primary classification aerosol regime distribution is SSP3-7.0 (Fig. 2f), however there are some key differences between SSP3-
7.0 and REF-2015. Parts of western Europe, for example, shift from the continental level 1 regime (regime 1) to the background
regime (regime 0), which can be interpreted as a consequence of emission reduction policies adopted by developed countries
in this scenario (Fujimori et al., 2017). Developing countries like China and India, on the contrary, are still characterized by
high levels of pollution in 2050, resulting in an increase in the extension of the continental level 3 and level 4 regimes (regime
315   8 and regime 2, respectively). Our results suggest that SSP2-4.5 and SSP3-7.0 are less probable to feature preindustrial
conditions than SSP1-1.9, although preindustrial conditions can be expected in these scenarios for specific regions, like the
ones covered by the background regime, marine regime and continental level 1 regime (Fig. 2e, f).

Our results show that close-to-preindustrial conditions exist in present-day and under SSP1-1.9 to a greater spatial extent and preindustrial times show more diverse conditions than previous studies suggested. Possible reasons for these differences are discussed in the following: (1) many previous studies identified preindustrial-like conditions based on CCN concentration. Andreae (2007) suggested that by turning off anthropogenic emissions, the simulated CCN concentration over the continents agree with that over the southern oceans, with the CCN concentration ranging from 50 to 200 cm^{-3}. Hamilton et al. (2014) used model simulations to identify present-day atmospheric conditions that resemble PI, by estimating the occurrence of days with similar CCN concentrations between PI-1750 and 2000, suggesting that 90% of unperturbed regions occur in the Southern Hemisphere. In contrast to these studies, we consider an aggregated information from multiple aerosol properties (BC, mineral dust, sea salt, POM, ammonium, sulfate, nitrate, particle number in Aitken mode, and particle number in Accumulation mode). However, as CCN concentrations are strongly related to some of these aerosol properties, our results can be compared to those from previous CCN-related studies qualitatively; (2) we are evaluating multi-annual mean aerosol properties, while other studies considered seasonal (Andreae, 2007) and daily variations (Hamilton et al. 2014), which could lead to larger differences between preindustrial and present-day than the differences we find using multi-annual means. Therefore, previous studies might have identified a smaller extent of preindustrial-like conditions than our study because more regions on Earth are considered to be different when using daily and seasonal data; (3) our results are based on ML-algorithms, which allow us to identify and characterize the complex relationships and patterns within the data based on similarities and differences in the global distribution of a multitude of aerosol properties, which is a major methodical difference to the previous studies.

The above results from the primary classification show the ability of the algorithm to extract a clear and condensed picture of the global distribution of aerosol conditions for different time periods and regions. Still, there are features that cannot be captured at the spatial scale of the primary classification. For example, in the L22 study, which used a higher spatial model resolution (i.e. T63, corresponding to 1.9°×1.9° in latitude and longitude) for the input dataset, the K-means algorithm could identify a north-south hemispheric difference for the marine regime, with a higher level of pollution in the Northern Hemisphere, but this difference is not evident in the present study, which uses a lower resolution (T42, 2.8°×2.8°). Such differences, however, would be a key information to constrain aerosol forcing uncertainties (e.g. Carslaw et al. 2014, Hamilton et al. 2014, Regayre et al. 2020). The absence of this north/south contrast suggests that our primary classifications are spatially too coarse and that a finer spatial clustering is required. This is achieved by means of a secondary classification, mostly targeting the regimes with low levels of aerosol identified by the primary classification.

3.2 Secondary classification of aerosol regimes and their properties

For the secondary classification shown in Figures 4 to 6 we target the following primary classification aerosol regimes: 1) the background regime, 2) the marine regime, and 3) the continental level 1 regime. These regimes are characterized by aerosol properties with much lower values than the other regimes (Fig. 2) and are therefore particularly important in preindustrial times

and in the SSP1-1.9 scenario, where they cover most of the areas of the globe. The aim of the secondary classification is to zoom into these specific primary regimes to identify further differences and similarities within these regimes. We refer to the regimes characterized by the secondary classification as "sub-regimes" and aim to answer the following question "Where do preindustrial-like aerosol conditions most probably occur at present-day and in the different future scenarios?

355

The sub-regime distributions of the background regime (Fig. 4) reveals that preindustrial-like aerosol conditions over the polar regions in both hemispheres can be found also in the present-day case and that aerosol conditions of large parts of the continents in the Northern Hemisphere during pre-industrial times can still be found under present-day conditions, but only at very high northern latitudes (i.e., the border between continents and the Arctic ocean). The secondary classification identifies 5 sub-

360 regimes within the present-day background regime: one with enhanced sea salt over the oceans (sub-regime 0_0), one in the Arctic with the second lowest aerosol values (sub-regime 0_1), one in the Antarctic with lowest aerosol values (sub-regime 0_2), a dust-enhanced one at the southern edge of Australia (sub-regime 0_3), and one over the continental boundaries of the Northern Hemisphere with the highest aerosol values (sub-regime 0_4). During preindustrial times, the northern polar region shows higher aerosol values than the south pole region, consistent with the present-day case. The Antarctic sub-regime has the

365 same extension in the preindustrial and in the present-day case, while the North Pole region sub-regime is larger than at present-day. Other continental regions belong to the sub-regime with highest aerosol values. The sub-regime distribution for SSP3-7.0 (Fig. 4f) closely resembles the present-day conditions, while the results for SSP1-1.9 (Fig. 4d) are similar to the preindustrial PI-1850 patterns. SSP2-4.5 (Fig. 4e) shows an intermediate stage between SSP3-7.0 and SSP1-1.9.
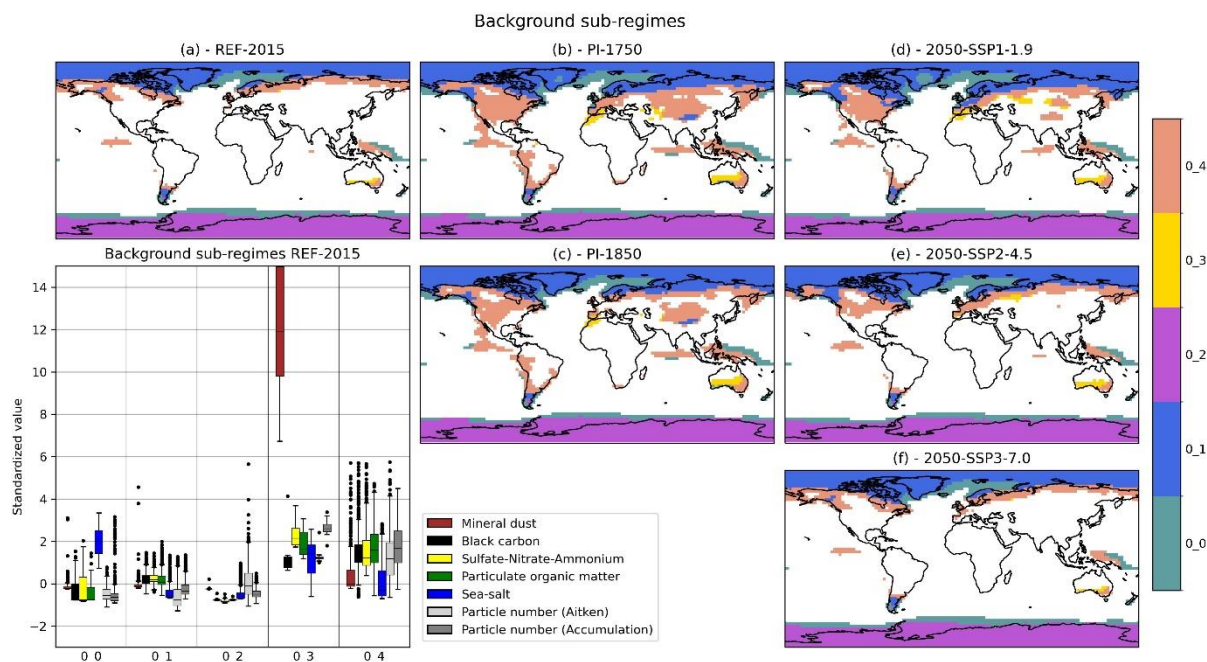
Figure 4: Results of the secondary classification for the background regime. The sub-regime distribution is shown for present-day (a), preindustrial times (b-c) and future (d-f). The aerosol properties for each regime of the present-day case are shown on the bottom left. Note that the standardized values here should not be directly compared with Fig. 3 and with other secondary classification results. The standardized value 0 of the secondary classifications represent the sample average of the target primary regime. The negative (positive) values describe data below (above) sample average expressed as factors of their sample standard deviation. Recall that the extension of the primary target regime (background) varies from case to case. Hence also the areas outside the target regime (white) vary.

Over the oceans, preindustrial-like conditions can only be found in the Southern Hemisphere (Fig. 5), as also pointed out by several previous studies and measurement campaigns (e.g. Andreae, 2007; Carslaw et al., 2014; Hamilton et al., 2014; McCoy et al., 2020). The present-day marine regime is further classified into three sub-regimes. The secondary classification (Fig. 5c) further identifies the different aerosol sub-regimes between the northern hemispheric (sub-regime 4_2) and the southern hemispheric oceans (sub-regime 4_0), with lower aerosol values in sub-regime 4_2 than 4_1. The marine regime contains a further sub-regime showing an enhancement in mineral dust, black carbon and POM at the outflow of the African continent (sub-regime 4_1) (Fig. 5d). This suggests that these sub-regimes are influenced by their neighbouring primary regimes to a certain extent, as a results of atmospheric long-range transport processes. In the preindustrial times and 2050 in SSP-1.9 scenario, the oceans are mostly classified into the sub-regimes 4_0, while only small regions in the tropics are identified as sub-regime 4_2. The reasons could be that aerosol conditions over the continents of the Northern Hemisphere in preindustrial times were not polluted enough to be able to influence the northern hemispheric oceans in a sufficient degree which can be recognized by the applied classification rules. The sub-regime 4_1 at the African outflow is consistent with the present-day

14

390   case. The distribution of sub-regimes of the marine regime is highly consistent between PI-1750 and PI-1850. The sub-regime distribution of SSP3-7.0 is almost identical with the present-day case, and SSP2-4.5 represents an intermediate stage between preindustrial times and present-day.
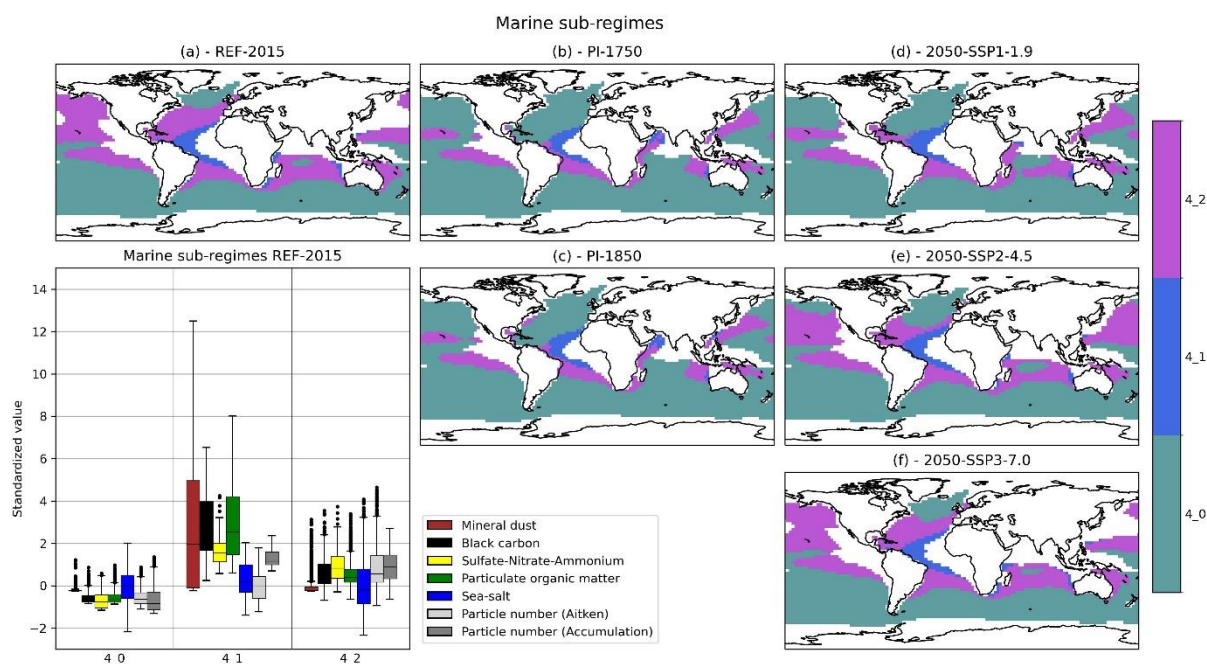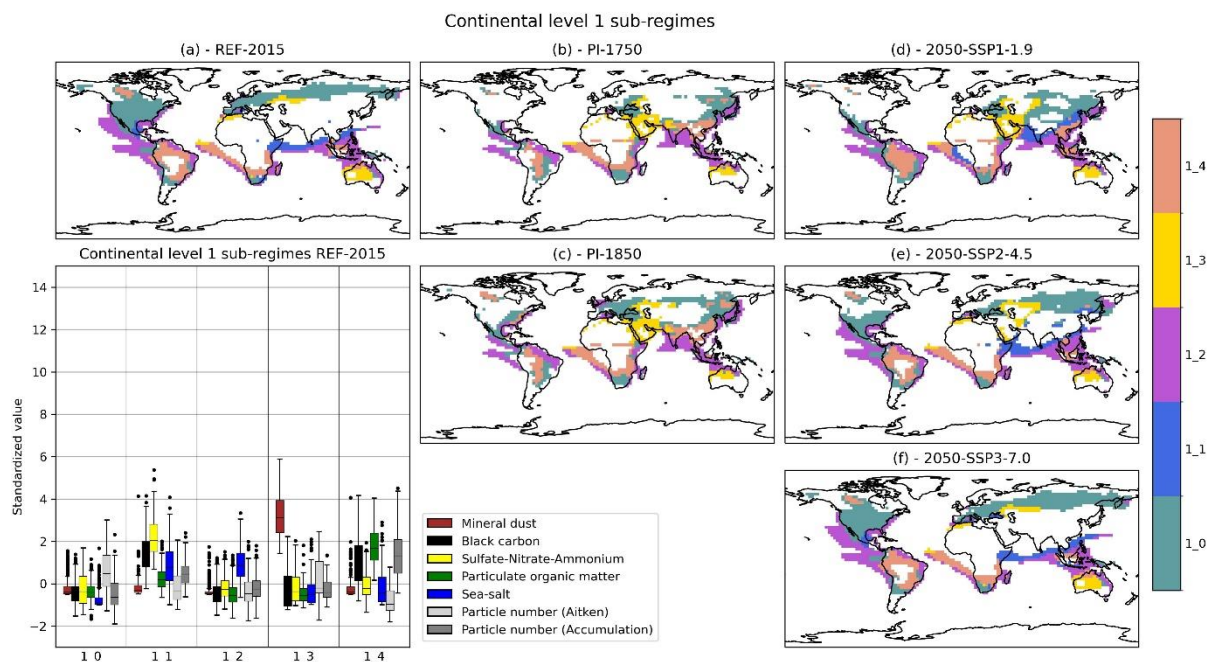

Figure 5: As in Fig. 4, but for the marine regime.

395

The sub-regimes of the continental level 1 regime show also locations were preindustrial-like conditions can be found in the present-day case (Fig. 6). The present-day continental level 1 regime contains a sub-regime 1_3 with dust enhancement, a sub-regime 1_2 with enhanced sea salt, a SNA-enhanced sub-regime 1_1 which is found at a latitudinal band across the oceans south of the Eurasian continent, a sub-regime 1_4 next to the primary biogenic regime, and a sub-regime 1_0 at northern

400   regions. In the preindustrial times, the regime shows a similar sub-regime structure as in the present-day, but fine differences occur. The present-day sub-regime 1_1 is not found during the preindustrial times, it seems to be replaced by the cleaner sub-regime 1_2. During preindustrial times, the dust enhanced sub-regime 1_3 has a larger spatial extent than in the present-day case, the biogenic/biomass burning enhanced sub-regime 1_4 includes also southeast China and parts of India which are the most polluted regions in the present-day case. The sub-regime 1_0 during preindustrial times corresponds to present-day

405   conditions in a few parts of North America and the Eurasian continent. Similar as the results for other secondary classification regimes, SSP3-7.0 closely resembles the present-day aerosol conditions, and SSP1-1.9 resembles PI-1850. SSP2-4.5 corresponds to an intermediate condition between preindustrial times and present-day.

15

Figure 6: As in Fig. 4, but for the continental level 1 regime.

3.2 Regional focus and emission analysis

The goal of this section is to explain prominent features of the temporal development by means of analysing the development of the emissions in selected regions. The results discussed in the previous sections allowed us to identify six representative regions within three groups (biogenic, most polluted region and developed countries) (Fig. 7a). Each group contains two regions which belong to the same aerosol regime during present-day, but follow different pathways in terms of their aerosol regime evolution from preindustrial times to the future. We investigate in this section how emission changes drive their regime development, by comparing the anthropogenic and biomass burning emissions of aerosol and precursor gases in the different time periods and scenarios for these regions (Fig. 7b-g). We consider three emission sectors (open burning, the sum of anthropogenic non-transport sectors, and the transport sector) and the sum of them. The transport sector includes land transport, shipping and aviation, with most of the emissions due to land transport. We consider four key species: NH_3 (mostly driven by agricultural activities), BC (representative for the emission from all kinds of combustion processes, including also open burning), SO_2 and NO_x (typical pollutants from fossil fuel combustion and both important for secondary aerosol formation). Most of the processes driving the anthropogenic aerosol changes will be addressed by the analysis of these species (Hoesly et al. 2018). The open burning sector comprises agricultural waste burning on fields, forest burning, grassland burning and peat burning (van Marle et al. 2017). The total emissions of each species are normalized with respect to their present-day total in each region, such that values of the total emissions larger (smaller) than 1 indicate an emission increase (decrease) with respect to the present-day.

16

Region R1a (over South America) and R1b (over Central Africa) are both identified as biogenic/biomass burning regimes

430 during present-day. While R1b belongs to the biogenic/biomass burning regime at all time periods, R1a belongs to continental level 1 regime during preindustrial times and seems to develop into the biogenic/biomass burning regime only in the present-day case (Fig. 2). This behavior can be explained by the emission analysis (Fig. 7b, c). Preindustrial emissions for R1a are very low (less than ~1% of present-day), while total preindustrial emissions for R1b are about 50-90% of the present-day value (depending on the species). This dramatic change in R1a between preindustrial and present-day conditions points to a strong

435 influence of human activities on the open burning emissions, e.g. due to deforestation. This also explains why the classification algorithm assigns R1a to a continental level 1 regime in the preindustrial time. In SSP1-1.9 the emissions in R1a amount to about 25-70% of the present-day value. The assignment of R1a to the continental level 1 regime under SSP1-1.9 suggests therefore that reducing ~50% of present-day emissions in R1a could reverse the direction of aerosol regime development in this region. R1a is barely influenced by open burning emissions in the preindustrial times, while this sector is a constant

440 emission source in R1b over the different time periods.

The south-east Asian regions R2a and R2b develop into the most polluted aerosol regimes on Earth in the present-day case. Both regions belong to the continental level 1 regime in the preindustrial times but develop differently in terms of their future regimes (Fig. 2) which can be explained by their slightly different emission pathways in the future scenarios (Fig. 7d, e). The

445 extremely low emissions during preindustrial times compared with the present-day result in large temporal differences in these regions. In 2050, R2a shows increased emissions of NO_x and NH_3 under the SSP3-7.0 and SSP2-4.5 scenarios. In R2a NO_x emissions increase by 30% for SSP2-4.5 and by 70% for SSP3-7.0 compared to the present-day case. An emission reduction can be seen for R2a under the clean scenario SSP1-1.9, with the exception of NH_3 which is strongly influenced by agricultural emissions. In R2b SSP3-7.0 still shows increases while SSP2-4.5 and SSP1-1.9 show decreasing emissions, except for NH_3,

450 again because of the persisting emissions from agriculture. The different pathways of emission changes in R2a and R2b can explain why R2a remains in the polluted regimes in 2050, while R2b shifts to a clean aerosol regime under SSP1-1.9. The transport sector has only small contributions for most species, except for NO_x. Compared to R2b, the relative contribution of the transport sector with respect to the total emissions is larger in R2a.

455 R3a and R3b are representative of developed countries and are covered by clean aerosol regimes. These regions show a gradual development from the background to the continental level 1 regime from past to present, and a reverse process from the present-day to the future (Fig. 2 and Fig. 6) under different degrees of emission reduction. The emission comparisons for both regions (Fig. 7f and g) show that the emission maxima of NO_x, SO_2 and BC occur at present-day, while emissions for NH_3 increase up to 20% in 2050 under the most pessimistic SSP3-7.0 scenario. However, the maximum aerosol emissions generally peak at

460 present-day. This trend agrees with the temporal development of the corresponding aerosol regimes. The anthropogenic non-

transport sector shows the largest contribution to the total emissions in these regions, followed by the contributions from the transport sector.
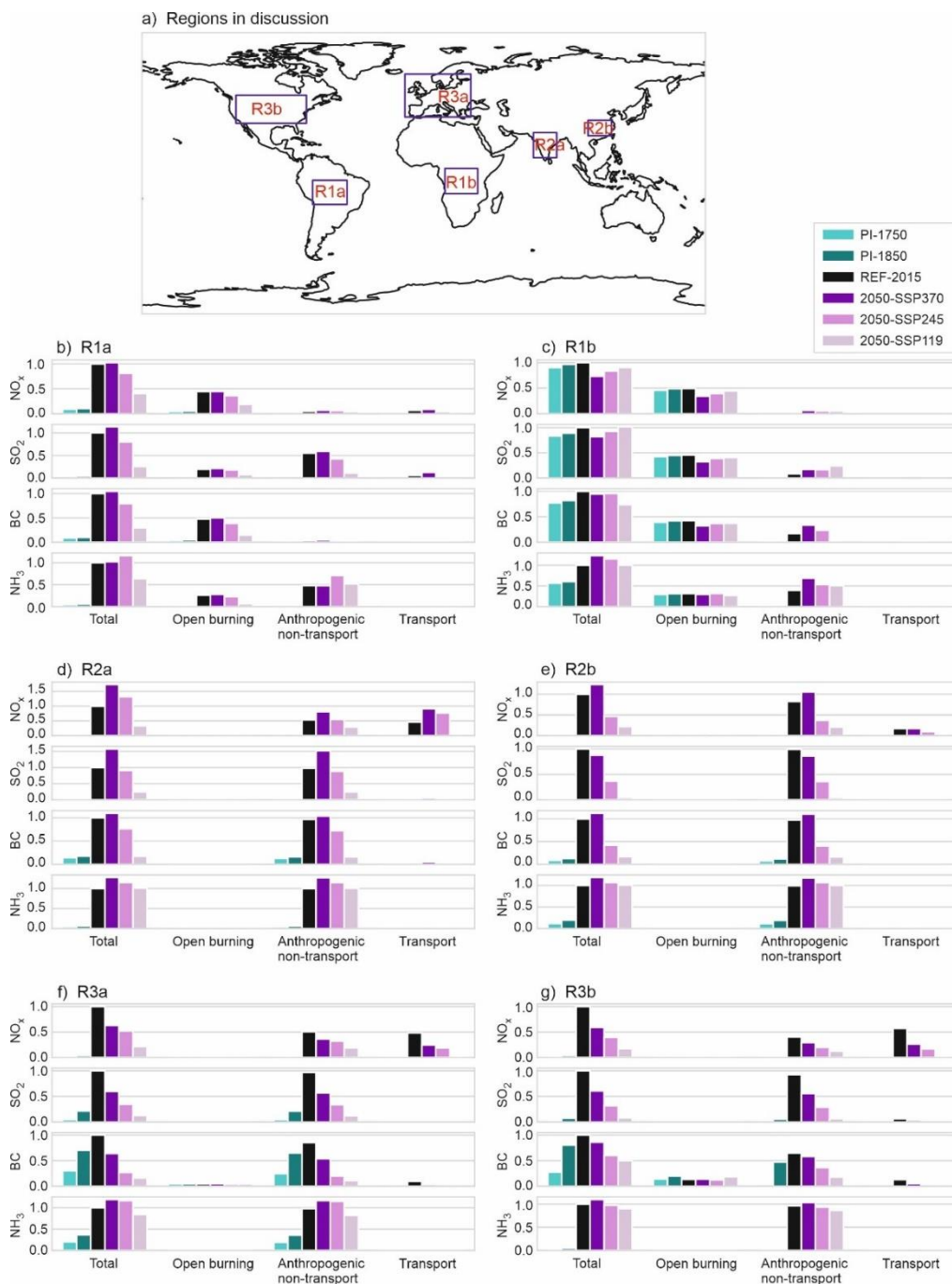
Figure 7: a) shows the six regions selected for the emission analysis, and b)-g) show the comparison of emissions for four species and from different sectors during different time and scenarios for each region. The emission amounts of each species are normalized to their present-day total. Note the different vertical scales in panel (d).

4 Limitations, strengths and potential applications

In order to set the results presented above in the right context we discuss the most important limitations, strengths and potential applications of our analysis in the following.

470

As already stated in L22, the classification algorithm is applied to the output of global model simulations and therefore cannot capture small-scale patterns (small-scale effects of individual pollution sources as, for instance, local plumes of specific roads, power plants, ships or oil platforms) due to the model's coarse resolution (~300 km in this study). Therefore, the presented results only consider large-scale patterns. In spite of this limitation, a clear advantage of using model-generated output is the

475 large number of aerosol properties calculated in a self-consistent manner as well as the complete spatio-temporal coverage of the globe for multi-annual time periods. This, to some extent, compensates for the limitations mentioned above and the uncertainties of global aerosol models identified by comparing to observations. Of course, model simulations can be affected by biases visible as deviations from measurements. This, however, is less critical in the context of this study, due to the standardization process. The classification algorithm is based on assessing large-scale distribution patterns of aerosol

480 properties and previous studies showed that these patterns are usually well captured by global models (Koch et al., 2009; Mann et al., 2014; Aquila et al., 2011; Koffi et al., 2015; Kaiser et al., 2019; Beer et al., 2020).

Another limitation specific to this study is related to the set-up of the model simulations, which considers time-varying emissions under fixed present-day climatic conditions. Although the intention of this study is to purely investigate the influence

485 of emissions on the development of aerosol regimes over time, the simulations for the preindustrial times and the future may not be fully representative of their atmospheric conditions in the real world. Changing emissions and climate simultaneously is technically possible and would not affect the algorithm skills, but it would hamper the separation of their respective impacts, further complicating the interpretation of results and the applicability of the proposed method. The investigation of the influence of both climate and emission changes on the temporal development of aerosol regimes may nevertheless be the

490 subject of a future study. Additionally, all our conclusions are driven by simulations using the adopted emission inventories. As stated above, these emission inventories might miss important emission phenomena, especially those occurring on small spatial and short temporal scales. However, on the climatological time scales analysed in this study, these limitations are not expected to change the conclusions. On the other hand, since we analyse long term mean conditions, the analysis cannot capture the fact that some areas may be subject to temporary pollution events (e.g., due to wild fires).

495 The analysis procedures developed in this study and the presented results are unique and have a large application potential. This combination of unsupervised and supervised machine learning methods is valuable for comparing consistent patterns across different datasets without knowing the a priori classification criteria. The application of this method is not limited to global aerosol simulations, but can be applied to different modelling and measurement (such as Satellite) datasets regardless of their resolution and spatial coverage. The clear and concise depiction of the spatial extent and distribution of aerosol regimes

500 for different time periods and emission scenarios is particularly useful. First, previous campaigns targeting preindustrial aerosol
conditions took place mainly over the southern oceans. Our results point to additional areas with aerosol conditions similar to
those at preindustrial times (such as the background regime, the biogenic regime in central Africa and the continental level 1
regime), which may be taken into consideration. Second, the representation of aerosol conditions for present-day and different
future scenarios, derived from a huge and complex dataset, provides insights for policy- and decision-makers on possible future
505 developments of atmospheric pollution. Third, the classification of aerosol conditions into regimes provides important hints
for subsequent studies relying on information about the properties and distribution of atmospheric aerosols. For example, these
regimes can be used as input for assessing the aging of aircraft engines dependent on atmospheric environmental conditions.
Many aerosol components (e.g. sea salt, mineral dust, black carbon, sulphate) induce highly relevant engine aging processes,
for instance through corrosion or abrasion (Ellis et al. 2021). Hence, detailed knowledge on aerosol characteristics in specific
510 regions is an important prerequisite for robust engine life cycle modelling. Our study addresses aerosol climatological
conditions in a similar manner as the IPCC does when defining climate reference regions (Iturbide et al. 2020). Iturbide et al.
(2020) defined 46 land and 16 ocean regions to represent consistent and climatically-coherent regional climate features based
on observational and model-simulated temperature and precipitation data, in order to provide climatological information for a
broad spectrum of IPCC users. Similarly, different communities (e.g., industry, policy, research) might benefit from the
515 aggerated aerosol information provided in our study.

5 Summary and outlook

This study investigates the temporal evolution of global aerosol regimes driven by emission changes, based on combining
results from global aerosol simulations with machine learning algorithms for different time periods and emission scenarios,
ranging from year 1750 to 2050. The investigations are conducted for the primary classification of aerosol regimes and a
520 secondary classification of more detailed structures in selected aerosol regimes. The results led to the following new findings
about aerosol patterns and their evolution:

(1)   The machine learning classification based on the present-day dataset (2015) (Fig. 2a and 3) identifies eight
aerosol regimes in the primary classification step: background, marine, biogenic/biomass burning, two dust-
525   dominated regimes that we combine into one, and four continental regimes with different levels of aerosol burden
(level 1 to level 4 characterized by increasing aerosol burden from level to level). During preindustrial times
(years 1750 and 1850), clean aerosol regimes (background, marine, and continental level 1) dominate, except for
mineral dust regimes in northern Africa and biomass burning/biogenic regimes in central southern Africa. The
aerosol regimes for 2050 under SSP3-7.0 closely resemble present-day conditions, but there are some notable
530   regional differences: developed countries tend to shift towards cleaner regimes in future, while the opposite is
the case for developing countries. The aerosol regimes for 2050 under SSP2-4.5 and SSP1-1.9 develop towards

20

cleaner aerosol conditions with respect to the present-day case, whereas SSP1-1.9 has the highest probability to resemble preindustrial conditions, more similar to PI-1850 than PI-1750. SSP2-4.5 mostly corresponds to an intermediate state between present-day and preindustrial times.

535 (2) A secondary classification was conducted in order to characterize the clean aerosol regimes in more detail (Figs. 4-6). The results suggest that present-day northern polar regions show a higher level of aerosol pollution than the southern polar regions, and this tendency is also evident in the preindustrial times. Present-day marine regimes show a north/south contrast, while preindustrial marine regimes mostly represent cleaner marine conditions found over the present-day southern oceans.

540 (3) An analysis of the emissions of aerosols and aerosol precursor gases was performed targeting six representative regions for three groups (biogenic, most polluted regions and developed countries). Regions within a specific group belong to the same regime during present-day, but follow different pathways in terms of their evolution over time. This behaviour can be interpreted in terms of regional changes in emissions through time. Prominent examples are: i) the biogenic/biomass burning regime over South America that is not present during pre-industrial
545 times since the emissions account for less than ~1% of present-day emissions; ii) the most polluted present-day regime in India, which shows a slower transition towards less polluted conditions than the corresponding regime in south-eastern China in 2050 for SSP1-1.9 and SSP2-4.5 due to different emission reduction policies; and iii) the developed countries where emission reductions also explain a shift towards preindustrial-like conditions in 2050 for all scenarios.

550

The results presented in this study can provide important insights for different communities (e.g., industry, policy, research). For instance, our findings can be used for the planning of targeted measurements for specific aerosol conditions (e.g. preindustrial-like, most polluted, biogenic/biomass burning), for supplying information to policy makers for tailored air pollution mitigation measures in specific regions, for model inter-comparisons (e.g. AeroCom, Gliss et al. 2021; AerChemMIP,
555 Collins et al. 2017) and for subsequent studies determining which aerosol conditions should be considered (e.g. life cycle modeling of aerosol engine).

For the applicability of the methods discussed in this work, a few caveats and limitations need to be considered. First, the global aerosol simulations are capable of capturing large-scale aerosol distribution patterns, but are not able to resolve small-
560 scale and localized processes. Therefore, these results consider solely large-scale patterns. Second, the atmospheric aerosol for preindustrial and future conditions is simulated by varying the emissions for the respective time period but with a fixed climate. With this approach we focus on the investigation of the influence of emission changes on aerosol regime development. The consideration of both climate and emission changes for the corresponding time periods could be the subject of a follow-up study.

565

The method we outlined here could also be applied to analyse the development of upper tropospheric aerosol regimes over time. This region is of particular interest for many areas of research, such as aviation climate impacts and volcanic emissions.

Data availability

The output of the model simulations investigated in this paper is available at https://doi.org/10.5281/zenodo.8134336 (Righi, 2023). The aggregated data generated in this study will be made available via doi in the final version of this paper.

Author contributions

JL conceived the study, developed and implemented the analyses procedures, analysed the data, and wrote the paper. MR performed the simulations used in this study. JH and AS supervised this study. MR, JH, CGB, UB and AS contributed to conceiving the study, interpreting the results, and writing the text.

Competing interests

The contact author has declared that none of the authors has any competing interests.

References

Andreae, M. O., Jones, C. D. and Cox, P. M.: 2005 Strong present-day aerosol cooling implies a hot future, Nature, 435, 1187-1190, doi: 10.1038/nature0367, 2005.

Andreae M. O.: Aerosols before pollution, Nature, 315, 50-51, doi:10.1126/science.1136529, 2007.

Aquila, V., Hendricks, J., Lauer, A., Riemer, N., Vogel, H., Baumgardner, D., Minikin, A., Petzold, A., Schwarz, J. P., Spackman, J. R., Weinzierl, B., Righi, M. and Dall'Amico, M.: MADE-in: a new aerosol microphysics submodel for global simulation of insoluble particles and their mixing state, Geosci. Model Dev., 4, 325–355, doi:10.5194/gmd-4-325-2011, 2011.

Beer, C. G., Hendricks, J., Righi, M., Heinold, B., Tegen, I., Groß, S., Sauer, D., Walser, A. and Weinzierl, B.: Modelling mineral dust emissions and atmospheric dispersion with MADE3 in EMAC v2.54, Geosci. Model Dev., 13, 4287-4303, doi:10.5194/gmd-13-4287-2020, 2020.

Bellouin, N., Quaas, J., Gryspeerdt, E., Kinne, S., Stier, P., WatsonParris, D., Boucher, O., Carslaw, K. S., Christensen, M., Daniau, A.-L., Dufresne, J.-L., Feingold, G., Fiedler, S., Forster, P., Gettelman, A., Haywood, J. M., Lohmann, U., Malavelle, F., Mauritsen, T., McCoy, D. T., Myhre, G., Mülmenstädt, J., Neubauer, D., Possner, A., Rugenstein, M., Sato, Y., Schulz, M., Schwartz, S. E., Sourdeval, O., Storelvmo, T., Toll, V., Winker, D. and Stevens, B.: Bounding global aerosol radiative forcing of climate change, Rev. Geophys., 58, e2019RG000660, doi:10.1029/2019RG000660, 2020.

Breiman, L.: Random Forest, Machine Learning, 45, 5-32, 2001.

Borge, R., Jung, D., Lejarraga, I., de la Paz, D. and Cordero, J. M.: Assessment of the Madrid region air quality zoning based on mesoscale modelling and K-means clustering, Atmos. Env., 287, 119258, doi: 10.1016/j.atmosenv.2022.119258, 2022.

Boucher, O., Randall, D., Artaxo, P., Bretherton, C., Feingold, G., Forster, P., et al.: Clouds and aerosols, In: Stocker TF, Qin, D., Plattner, G.-K., Tignor, M., Allen, S. K., Boschung, J., Nauels, A., Xia, Y., Bex, V., Midgley, P. M., editors. Climate change 2013: the physical science basis contribution of Working Group I to the Fifth Assessment Report of the Intergovernmental Panel on Climate Change. Cambridge, United Kingdom and New York, NY, USA: Cambridge University Press. p. 571. 2013

Carslaw, K. S., Lee, L. A., Reddington, C. L., Pringle, K. J., Rap, A., Forster, P. M., Mann, G. W., Spracklen, D. V., Woodhouse, M. T., Regaryre, L. A. and Pierce, J. R.: Large contribution of natural aerosols to uncertainty in indirect forcing, Nature, 503, 67-71, doi:10.1038/nature12674, 2013.

Carslaw, K. S., Gordon, H., Hamilton, D. S., Johnson, J. S., Regayre, L. A., Yoshioka, M. and Pringle, K. J.: Aerosol in the pre-industrial atmosphere, Curr. Clim. Change Rep., 3, 1-15, doi:10.1007/s40641-017-0061-2, 2017.

Choi, W., Kang, H., Shin, D. and Lee, H.: Satellite-based aerosol classification for capital cities in Asian using a random forest model, Remote Sens., 13, 2464, doi:10.3390/rs13132464, 2021.

Christopoulos, C. D., Garimella, S., Zawadowicz, M. A., Möhler, O. and Cziczo, D. J.: A machine learning approach to aerosol classification for single-particle mass spectrometry, Atmos. Meass. Tech., 11, 5687-5699, doi: 10.5194/amt-11-5687-2018, 2018.

Collins, W. J., Lamarque, J.-F., Schulz, M., Boucher, O., Eyring, V., Hegglin, M., Maycock, A., Myhre, G., Prather, M., Shindell, D. and Smith, S. J.: AerChemMIP: quantifying the effects of chemistry and aerosols in CMIP6, Geosci. Model Dev., 10, 585–607, doi:10.5194/gmd-10-585-2017, 2017.

23

630 Dee, D. P., Uppala, S. M., Simmons, A. J., Beerisford, P., Poli, P., Kobayashi, S., Andrae, U., Balmaseda, M. A., Balsamo, G., Bauer, P., Bechtold, P., Beljaars, A. C. M., van der Berg, L., Bidlot, J., Bormann, N., Delsol, C., Dragani, R., Fuentes, M., Geer, A. J., Haimberger, L., Healy, S. B., Hersbach, H., Holm, E. V., Isaksen, L., Kallberg, P., Köhler, M., Matricardi, M., McNally, A. P., Monge-Sanz, B. M., Morcrette, J.-J., Park, B.-K., Peubey, C., de Rosnay, P., Tavolato, C., Thepaut, J.-N. and Vitart, F.: The ERA Interim reanalysis: Configuration and performance of the data assimilation system, Q. J.
635 Roy. Meteorol. Soc., 137, 553–597, doi:10.1002/qj.828, 2011.

Ellis, M., Bojdo, N., Filippone, A. and Clarkson, R.: Monte Carlo Predictions of Aero-Engine Performance Degradation Due to Particle Ingestion, Aerospace, 8, 146, doi:10.3390/aerospace8060146, 2021.

Feng, L., Smith, S. J., Braun, C., Crippa, M., Gidden, M. J., Hoesly, R., Klimont, Z., van Marle, M., van den Berg, M. and van der Werf, Guido. R.: The generation of gridded emissions data for CMIP6, Geosci. Model Dev., 13, 461–482,
640 doi:10.5194/gmd-13-461-2020, 2020.

Fricko, O., Havlik, P., Rogelj, J., Klimont, Z., Gusti, M., Johnson, N., Kolp, P., Strubegger, M., Valin, H., Amann, M., Ermolieva, T., Forsell, N., Herrero, M., Heyes, C., Kindermann, G., Krey, V., McCollum, D. L., Obersteiner, M., Pachauri, S., Rao, S., Schmid, E., Schoepp, W. and Riahi, K.: The marker quantification of the Shared Socioeconomic Pathway 2: A middle-of-the-road scenario for the 21st century, Global Environ. Change, 42, 251–267,
645 doi:10.1016/j.gloenvcha.2016.06.004, 2017.

Fujimori, S., Hasegawa, T., Masui, T., Takahashi, K., Herran, D. S., Dai, H., Hijioka, Y. and Kainuma, M.: SSP3: AIM implementation of Shared Socioeconomic Pathways, Global Environ. Change, 42, 268–283, doi:10.1016/j.gloenvcha.2016.06.009, 2017.

Gidden, M. J., Riahi, K., Smith, S. J., Fujimori, S., Luderer, G., Kriegler, E., van Vuuren, D. P., van den Berg, M., Feng, L.,
650 Klein, D., Calvin, K., Doelman, J. C., Frank, S., Fricko, O., Harmsen, M., Hasegawa, T., Havlik, P., Hilaire, J., Hoesly, R., Horing, J., Popp, A., Stehfest, E. and Takahashi, K.: Global emissions pathways under different socioeconomic scenarios for use in CMIP6: a dataset of harmonized emissions trajectories through the end of the century, Geosci. Model Dev., 12, 1443-1475, doi: 10.5194/gmd-12-1443-2019, 2019.

Gliß, J., Mortier, A., Schulz, M., Andrews, E., Balkanski, Y., Bauer, S. E., Benedictow, A. M. K., Bian, H., Checa-Garcia, R.,
655 Chin, M., Ginoux, P., Griesfeller, J. J., Heckel, A., Kipling, Z., Kirkevåg, A., Kokkola1, H., Laj, P., Le Sager, P., Lund, M. T., Myhre, C. L., Matsui, H., Myhre, G., Neubauer, D., van Noije, T., North, P., Olivié, D. J. L., Rémy, S., Sogacheva, L., Takemura, T., Tsigaridis, K. and Tsyro, S. G.: AeroCom phase III multi-model evaluation of the aerosol life cycle and optical properties using ground- and space-based remote sensing as well as surface in situ observations, Atmos. Chem. Phys., 21, 87–128, doi:10.5194/acp-21-87-2021, 2021.

660 Gryspeerdt, E., Povey, A. C., Grainger, R. G., Hasekamp, O., Hsu, N. C., Mulcahy, J. P., Sayer, A. M. and Sorooshian, A.: Uncertainty in aerosol–cloud radiative forcing is driven by clean conditions, Atmos. Chem. Phys., 23, 4115–4122, doi:10.5194/acp-23-4115-2023, 2023.

Guelle, W., Schulz, M., Balkanski, Y. and Dentener, F.: Influence of the source formulation on modeling the atmospheric global distribution of sea salt aerosol, J. Geophys. Res.-Atmos., 106, 27509–27524, doi:10.1029/2001JD900249, 2001.

665 Hamilton, D. S., Lee, L. A., Pringle, K. J., Reddington, C. L., Spracklen, D. V. and Carslaw, K. S.: Occurrence of pristine aerosol environments on a polluted planet, PNAS, 30, 18466-18471, doi:10.1073/pnas.1415440111, 2014.

Hartigan, J. A. and Wong, M. A.: Algorithm AS 136: A k-Means Clustering Algorithm, J. Royal Stat. Soc., 28, 100–108, doi:10.2307/2346830, 1979.

Hastie, T., Tibshirani, R. and Friedman, J.: The elements of statistical learning (2nd ed.), Springer, ISBN 0-387-95284-5, 2008.

670 Hawkins, E, Ortega, P, Suckling, E, Schurer, A, Hegerl, G, Jones, P, et al.: Estimating changes in global temperature since the preindustrial period, Bulletin of the American Meteorological Society, 1841-1856, BAMS–D–16–0007.1, 2017.

Hoesly, R. M., Smith, S. J., Feng, L., Klimont, Z., Janssens-Maenhout, G., Pitkanen, T., Seibert, J. J., Vu, L., Andres, R. J., Bolt, R. M., Bond, T. C., Dawidowski, L., Kholod, N., Kurokawa, J., Li, M., Liu, L., Lu, Z., Moura, M. C. P., O'Rourke, P. R. and Zhang, Q.: Historical (1750-2014) anthropogenic emissions of reactive gases and aerosols from the Community

675 Emissions Data System (CEDS), Geosci. Model. Dev., 11, 369-408, doi:10.5194/gmd-11-369-2018, 2018.

IPCC, 2021: Climate Change 2021: The Physical Science Basis. Contribution of Working Group I to the Sixth Assessment Report of the Intergovernmental Panel on Climate Change, [Masson-Delmotte, V., Zhai, P., Pirani, A., Connors, S.L., Péan, C., Berger, S., Caud, N., Chen, Y., Goldfarb, L., Gomis, M.I., Huang, M., Leitzell, K., Lonnoy, E., Matthews, J.B.R., Maycock, T.K., Waterfield, T., Yelekçi, O., Yu, R., and Zhou, B. (eds.)]. Cambridge University Press, Cambridge, United

680 Kingdom and New York, NY, USA, In press, doi:10.1017/9781009157896.

IPCC. Global Warming of 1.5∘C: IPCC Special Report on Impacts of Global Warming of 1.5∘C above Pre-Industrial Levels in Context of Strengthening Response to Climate Change, Sustainable Development, and Efforts to Eradicate Poverty, 1st ed.; Cambridge University Press: Cambridge, UK, 2022.

Iturbide, M., Gutiérrez, J. M., Alves, L. M., Bedia, J., Cerezo-Mota, R., et al.: An update of IPCC climate reference regions

685 for subcontinental analysis of climate model data: definition and aggregated datasets, Earth Syst. Sci. Data, 12, 2959–2970, doi:10.5194/essd-12-2959-2020, 2020.Jöckel, P., Kerkweg, A., Pozzer, A., Sander, R., Tost, H., Riede, H., Baumgaertner, A., Gromov, S. and Kern, B.: Development cycle 2 of the Modular Earth Submodel System (MESSy2), Geosci. Model Dev., 3, 717–752, doi:10.5194/gmd-3-717-2010, 2010.

Jöckel, P., Tost, H., Pozzer, A., Kunze, M., Kirner, O., Brenninkmeijer, C. A. M., Brinkop, S., Cai, D. S., Dyroff, C., Eckstein,

690 J., Frank, F., Garny, H., Gottschaldt, K.-D., Graf, P., Grewe, V., Kerkweg, A., Kern, B., Matthes, S., Mertens, M., Meul, S., Neumaier, M., Nützel, M., Oberländer-Hayn, S., Ruhnke, R., Runde, T., Sander, R., Scharffe, D., and Zahn, A.: Earth System Chemistry integrated Modelling (ESCiMo) with the Modular Earth Submodel System (MESSy) version 2.51, Geosci. Model Dev., 9, 1153–1200, doi:10.5194/gmd-9-1153-2016, 2016.

Kaiser, J. C., Hendricks, J., Righi, M., Riemer, N., Zaveri, R. A., Metzger, S. and Aquila, V.: The MESSy aerosol submodel

695 MADE3 (v2.0b): description and a box model test, Geosci. Model Dev., 7, 1137–1157, doi:10.5194/gmd-7-1137-2014, 2014.

Kaiser, J. C., Hendricks, J., Righi, M., Jöckel, P., Tost, H., Kandler, K., Weinzierl, B., Sauer, D., Heimerl, K., Schwarz, J. P., Perring, A. E. and Popp, T.: Global aerosol modeling with MADE3(v3.0) in EMAC (basedonv2.53): model description and evaluation, Geosci. Model Dev., 12, 541–579, doi:10.5194/gmd-12-541-2019, 2019.

700   Kianian, B., Liu, Y. and Chang, H. H.: Satellite-derived aerosol optical depth using a multi-resolution spatial model and random forest for PM2.5, prediction Remote Sens., 13, 126, doi: 10.3390/rs13010126, 2021.

Koch, D., Schulz, M., Kinne, S., McNaughton, C., Spackman, J. R., Balkanski, Y., Bauer, S., Berntsen, T., Bond, T. C., Boucher, O., Chin, M., Clarke, A., De Luca, N., Dentener, F., Diehl, T., Dubovik, O., Easter, R., Fahey, D. W., Feichter, J., Fillmore, D., Freitag, S., Ghan, S., Ginoux, P., Gong, S., Horowitz, L., Iversen, T., Kirkevåg, A., Klimont, Z., Kondo,

705   Y., Krol, M., Liu, X., Miller, R., Montanaro, V., Moteki, N., Myhre, G., Penner, J. E., Perlwitz, J., Pitari, G., Reddy, S., Sahu, L., Sakamoto, H., Schuster, G., Schwarz, J. P., Seland, Ø., Stier, P., Takegawa, N., Takemura, T., Textor, C., van Aardenne, J. A. and Zhao, Y.: Evaluation of black carbon estimations in global aerosol models, Atmos. Chem. Phys., 9, 9001–9026, doi:10.5194/acp-9-9001-2009, 2009.

Koffi, B, Szopa, S., Cozic, A., Hauglustaine, D. and van Velthoven, P.: Present and future impact of aircraft, road traffic and

710   shipping emissions on global tropospheric ozone, Atmos. Chem. Phys., 10, 11681-11705, doi:10.5194/acp-10-11681-2010, 2010.

Koffi, B., Schulz, M., Bréon, F.-M., Dentener, F., Steensen, B. M., Griesfeller, J., Winker, D., Balkanski, Y., Bauer, S. E., Bellouin, N., Berntsen, T., Bian, H., Chin, M., Diehl, T., Easter, R., Ghan, S., Hauglustaine, D. A., Iversen, T., Kirkevåg, A., Liu, X., Lohmann, U., Myhre, G., Rasch, P., Seland, Ø., Skeie, R. B., Steenrod, S. D., Stier, P., Tackett, J., Takemura,

715   T., Tsigaridis, K., Vuolo, M. R., Yoon, J. and Zhang, K.: Evaluation of the aerosol vertical distribution in global aerosol models through comparison against CALIOP measurements: AeroCom phase II results, J. Geophys. Res.-Atmos., 121, 7245–7283, doi:10.1002/2015JD024639, 2015.

Kulmala, M., Asmi, A., Lappalainen, H. K., Baltensperger, U., et al.: General overview: European Integrated project on Aerosol Cloud Climate and Air Quality interactions (EUCAARI) – integrating aerosol research from nano to global scales,

720   Atmos. Chem. Phys., 11, 13061–13143, doi:10.5194/acp-11-13061-2011, 2011.

Lauer, A., Hendricks, J., Ackermann, I., Schell, B., Hass, H. and Metzger, S.: Simulating aerosol microphysics with ECHAM/MADE GCM Part I: Model description and comparison with observations, Atmos. Chem. Phys., 5, 3251-3276, 2005.

Lauer, A. and Hendricks, J.: Simulating aerosol microphysics with the ECHAM4/MADE GCM – Part II: Results from a first

725   multiannual simulation of the submicrometer aerosol, Atmos. Chem. Phys., 6, 5495–5513, doi: 10.5194/acp-6-5495-2006, 2006.

Lee, J., Shi, Y., Cai, C., Ciren, P., Wang, J., Gangopadhyay, A. and Zhang, Z.: Machine learning based algorithms for global dust aerosol detection from satellite images: Inter-comparisons and evaluation, Remote Sens., 13, 456, doi: 10.3390/rs13030456, 2021.

730 Li, J., Hendricks, J., Righi, M. and Beer, C. G.: An aerosol classification scheme for global simulations using the K-means machine learning method, Geosci. Model Dev., 15, 509-533, doi: 10.5194/gmd-15-509-2022, 2022.

Liaw, A and Wiener, M: Classification and regression by random forest, R news, 2, 18-222002.

MacQueen, J. B.: Some Methods for classification and Analysis of Multivariate Observations. Proceedings of 5th Berkeley Symposium on Mathematical Statistics and Probability. 1., University of California Press. pp. 281–297., MR 0214227, Zbl

735   0214.46201, Retrieved 2009-04-07, 1967.

Mann, G. W., Carslaw, K. S., Spracklen, D. V., Ridley, D. A., Manktelow, P. T., Chipperfield, M. P., Pickering, S. J. and Johnson, C. E.: Description and evaluation of GLOMAP-mode: a modal global aerosol microphysics model for the UKCA composition-climate model, Geosci. Model Dev., 3, 519–551, doi:10.5194/gmd-3-519-2010, 2010.

Mann, G. W., Carslaw, K. S., Reddington, C. L., Pringle, K. J., et al.: Intercomparison and evaluation of global aerosol

740   microphysical properties among AeroCom models of a range of complexity, Atmos. Chem. Phys., 14, 4679-4713, doi:10.5194/acp-14-4679-2014, 2014.

McCoy, I. L., McCoy, D. T., Wood, R., Regayre, L., Watson-Parris, D., Grosvenor, D. P., Mulcahy, J. P., Hu, Y., Bender, F. A.-M., Field, P. R., Carslaw, K. S. and Gordon, H.: The hemispheric contrast in cloud microphysical properties constrains aerosol forcing, PNAS, 117, 18998-19006, doi: 10.1073/pnas.1922502117, 2020.

745 Milligan, G. W. and Cooper, M. C.: A study of standardization of variables in cluster analysis, Journal of Classification, 5, 181-204, 1988.

Myhre, G., Aas, W., Cherian, R., Collins, W., Faluvegi, G., Flanner, M., Forster, P., Hodnebrog, Ø., Klimont, Z., Lund, M. T., Mülmenstädt, J., Lund Myhre, C., Olivié, D., Prather, M., Quaas, J., Samset, B. H., Schnell, J. L., Schulz, M., Shindell, D., Skeie, R. B., Takemura, T. and Tsyro, S.: Multi-model simulations of aerosol and ozone radiative forcing due to

750   anthropogenic emission changes during the period 1990–2015, Atmos. Chem. Phys., 17, 2709–2720, doi:10.5194/acp-17-2709-2017, 2017.

O'Neill, B. C., Kriegler, E., Ebi, K. L., Kemp-Benedict, E., Riahi, K., Rothman, D. S., van Ruijven, B. J., van Vuuren, D. P., Birkmann, J., Kok, K., Levy, M. and Solecki, W.: The roads ahead: Narratives for shared socioeconomic pathways describing world futures in the 21st century, Global Environ. Change, 42, 169–180, doi: 10.1016/j.gloenvcha.2015.01.004,

755   2017.

Pedregosa, F., Varoquaux, G., Gramfort, A., Michel, V., Thirion, B., Grisel, O., Blondel, M., Prettenhofer, P., Weiss, R., Dubourg, V., Vanderplas, J., Passos, A., Cournapeau, D., Brucher, M., Perrot, M. and Duchesnay, É.: Scikit-learn: Machine Learning in Python, JMLR, 12, 2825-2830, 2011.

Pringle, K. J., Tost, H., Message, S., Steil, B., Giannadaki, D., Nenes, A., Fountoukis, C., Stier, P., Vignati, E. and Lelieveld,

760   J.: Description and evaluation of GMXe: a new aerosol submodel for global simulations (v1), Geosci. Model Dev., 3, 391–412, doi:10.5194/gmd-3-391-2010, 2010.

Quaas, J., Jia, H., Smith, C., Albright, A. L., Aas, W., Bellouin, N., Boucher, O., Doutriaux-Boucher, M., Forster, P. M., Grosvenor, D., Jenkins, S., Klimont, Z., Loeb, N. G., Ma, X., Naik, V., Paulot, F. and Stier, P.: Robust evidence for reversal

of the trend in aerosol effective climate forcing, Atmos. Chem. Phys., 22, 12221–12239, doi:10.5194/acp-22-12221-2022, 2022.

Quinlan, J. R.: Induction of decision trees, Machine Learning, 1, 81-106, 1986.

Quinlan, J. R.: Simplifying decision trees, International Journal of Man-Machine studies, 27, 221-234, doi: 10.1016/S0020-7373(87)80053-6, 1987.

Raudsepp, U. and Maljutenko, I.: A method for assenment of the general circulation model quality using the K-means clustering algorithm: a case study with GETM v2.5, Geosci. Model Dev., 15, 535-551, doi: 10.5194/gmd-15-535-2022, 2022.

Regayre, L. A., Schmale, J., Johnson, J. S., Tatzelt, C., Baccarini, A., Henning, S., Yoshioka, M., Stratmann, F., Gysel-Beer, M., Grosvenor, D. P. and Carslaw, K. S.: The value of remote marine aerosol measurements for constraining radiative forcing uncertainty, Atmos. Chem. Phys., 20, 10063-10072, doi: 10.5194/acp-20-10063-2020, 2020.

Righi, M., Hendricks, J., Lohmann, U. Beer, C. G., Hahn, V., Heinold, B., Heller, R., Krämer, M., Ponater, M., Rolf, C. Tegen, I. and Vogit, C.: Coupling aerosols to (cirrus) clouds in the global EMAC-MADE3 aerosol-climate model, Geosci. Model Dev., 13, 1635-1661, doi:10.5194/gmd-13-1635-2020, 2020.

Righi, M., Hendricks, J., and Brinkop, S.: The global impact of the transport sectors on the atmospheric aerosol and the resulting climate effects under the Shared Socioeconomic Pathways (SSPs), Earth Syst. Dynam., 14, 835–859, doi.:10.5194/esd-14-835-2023, 2023.

Rousseeuw, P. J.: Silhouettes: a graphical aid to the interpretation and validation of cluster analysis, Comput. Appl. Math., 20, 53-65, doi:10.1016/0377-0427(87)90125-7, 1987.

Schmale, J., Baccarini, A., Thurnherr, I., Henning, S., Efraim, A., Regayre, L., Bolas, C., Hartmann, M., Welti, A., Lehtipalo, K., Aemisegger, F., Tatzelt, C., Landwehr, S., Modini, R. L., Tummon,, F., Johnson, J. S., Harris, N., Schnaiter, M., Toffoli, A., Derkani, M., Bukowiecki, N., Stratmann, F. Dommen, J., Baltensperger, U., Wernli, H., Rosenfeld, D., Gyseleer, M. and Carslaw, K. S.: Overview of the Antarctic circumnavigation expedition: study of preindustrial-like aerosols and their climate effects (ACE-SPACE), BAMS, 100, 2260-2283, doi: 10.1175/BAMS-D-18-0187.1,.2019.

Sessions, W. R., Reid, J. S., Benedetti, A., Colarco, P. R., da Silva, A., Lu, S., Sekiyama, T., Tanaka, T. Y., Baldasano, J. M., Basart, S., Brooks, M. E., Eck, T. F., Iredell, M., Hansen, J. A., Jorba, O. C., Juang, H.-M. H., Lynch, P., Morcrette, J.-J., Moorthi, S., Mulcahy, J., Pradhan, Y., Razinger, M., Sampson, C. B., Wang, J. and Westphal, D. L.: Development towards a global operational aerosol consensus: basic climatological characteristics of the International Cooperative for Aerosol Prediction MultiModel Ensemble (ICAP-MME), Atmos. Chem. Phys., 15, 335–362, doi:10.5194/acp-15-335-2015, 2015.

Spencer, N. H.: 5.4.5 Squared Euclidean Distances, Essentials of Multivariate Data Analysis, CRC Press, p. 95, ISBN 9781466584792, 2013.

Tegen, I., Harrison, S. P., Kohfeld, K., Prentice, I. C., Coe, M. and Heimann, M: Impact of vegetation and preferential source areas on global dust aerosol: Results from a model study, J. Geophys. Res. - Atmos., 107, 4576, doi:10.1029/2001JD000963, 2002.

Tibshirani, R., Walther, G. and Hastie, T.: Estimating the number of clusters in a dataset via the gap statistic, J. R. Stat. Soc. Ser., B (Statistical Methodol.), 63, 411–423, 2001.

800 Thomason, L. W. and Vernier, J.-P.: Improved SAGE II cloud/aerosol categorization and observations of the Asian tropopause aerosol layer: 1989–2005, Atmos. Chem. Phys., 13, 4605–4616, doi:10.5194/acp-13-4605-2013, 2013.

Van Marle, M. J. E., Kloster, S., Magi, B. I., Marlon, J. R., Daniau, A.-L., Field, R. D., Arneth, A., Forrest, M., Hantson, S., Kehrwald, N. M., Knorr, W., Lasslop, G., Li, F., Mangeon, S., Yue, C., Kaiser, J. W., van der Werf, G. R.: Historic global biomass burning emissions for CMIP6(BB4CMIP) based on merging satellite observations with proxies and fire models 805 (1750-2015), Geosci. Model Dev., 10, 3329-3357, doi: 10.5194/gmd-10-3329-2017, 2017.

van Vuuren, D. P., Stehfest, E., Gernaat, D. E., Doelman, J. C., van den Berg, M., Harmsen, M., de Boer, H. S., Bouwman, L. F., Daioglou, V., Edelenbosch, O. Y., Girod, B., Kram, T., Lassaletta, L., Lucas, P. L., van Meijl, H., Müller, C., van Ruijven, B. J., van der Sluis, S. and Tabeau, A.: Energy, land-use and greenhouse gas emissions trajectories under a green growth paradigm, Global Environ. Change, 42, 237–250, doi:10.1016/j.gloenvcha.2016.05.008, 2017.

810 Vernier, H., Rastogi, N., Liu, H., Pandit, A. K., Bedka, K., Patel, A., Ratnam, M. V., Kumar, B. S., Zhang, B., Gadhavi, H., Wienhold, F., Berthet, G. and Vernier, J.-P.: Exploring the inorganic composition of the Asian Tropopause Aerosol Layer using medium-duration balloon flights, Atmos. Chem. Phys., 22, 12675-12694, doi: 10.5194/acp-22-12675-2022, 2022.

Wei, C.-L., Rowe, G. T., Escobar-Briones, E., Boetius, A., Soltwedel, T., Caley, M. J., Soliman, Y., Huettmann, F., Qu, F., Yu, Z., Pitcher, C. R., Haedrich, R. L., Wicksten, M. K., Rex, M. A., Baguley, J. W., Sharma, J., Danovaro, R., MacDonald, 815 I. R., Nunnally, C. C., Deming, J. M., Montagna, P., Levesque, M., Weslawski, J. M., Wlodarska-Kowalczuk, M., Ingole, B. S., Bett, B. J., billet, D. S. M., Yool, A., Bluhm, B. A., Iken, K., Narayanaswamy, B. E.: Global patterns and predictions of seafloor biomass using random forest, PLoS ONE, 5, (12), e15323, doi: 10.1371/journal.pone.0015323, 2010.

Xu, Y., Lamarque, J.-F. and Sanderson, B. M.: The importance of aerosol scenarios in projectons of future heat extremes, Climate Change, 146, 393-406, doi: 10.1007/s10584-015-1565-1, 2018.

820 Yu, F., Luo, G., Nair, A. A., Tsigaridis, K. and Bauer, S. E.: Use of machine learning to reduce uncertainties in particle number concentration and aerosol indirect radiative forcing predicted by climate models, Geophys. Res. Lett., 49, e2022GL098551 doi:10.1029/2022GL098551, 2022.

Zhao, A. Bollasina, M. A. and Stevenson, D. S.: Strong influences of aerosol reductions on future heatwaves, Geophys. Res. Lett., 46, 4913-4923, doi:10.1029/2019GL082269, 2019.

825